A synthesis dataset of permafrost thermal state for the Qinghai-Tibet (Xizang) Plateau, China

Lin Zhao[1,2*], Defu Zou[2], Guojie Hu[2*], Tonghua Wu[2], Erji Du[2], Guangyue Liu[2], Yao Xiao[2], Ren Li[2], Qiangqiang Pang[2], Yongping Qiao[2], Xiaodong Wu[2], Zhe Sun[2], Zanpin Xing[2], Yu Sheng[3], Yonghua Zhao[2], Jianzong Shi[2], Changwei Xie[2], Lingxiao Wang[1], Chong Wang[1], Guodong Cheng[2]

[1] School of Geographical Sciences, Nanjing University of Information Science & Technology, Nanjing 210044, China

[2] Cryosphere Research Station on Qinghai-Xizang Plateau, State Key Laboratory of Cryospheric Sciences, Northwest Institute of Eco-Environment and Resources, Chinese Academy of Sciences, Lanzhou 730000, China

[3] *State Key Laboratory of Frozen Soil Engineering, Northwest Institute of Eco-Environment and Resources, Chinese Academy of Sciences, Lanzhou 730000, China*

Correspondence: Lin Zhao (lzhao@nuist.edu.cn), Guojie Hu (huguojie123@lzb.ac.cn)

Abstract:

Permafrost is important for the climatic, hydrological, and ecological processes on the Qinghai-Tibet Plateau (QTP). The changing permafrost and its impact have been attracting great attention worldwide never before. More observational and modeling approaches are needed to promote an understanding of permafrost thermal state and climatic conditions on the QTP. However, limited data on the permafrost thermal state and climate background were sporadically reported in different pieces of literature due to the difficulties to access to and work in this region, where the weather is severe, environmental conditions are harsh and the topographic and morphological features are complex. From the 1990s, we began to establish the permafrost monitoring network on the QTP. Meteorological variables were measured by automatic meteorological systems. The soil temperature and moisture data were collected from an integrated observation system in the active layer. Deep ground temperature (GT) was observed from boreholes. In this study, a comprehensive dataset after quality control consisting of long-term meteorological, GT, soil moisture and soil temperature data were compiled from an integrated, distributed and multiscale observation network in the permafrost

regions of QTP. These datasets were helpful for the scientists with multiple study fields (i.e., climate, cryospheric, ecology and hydrology, meteorology science), which will significantly promote the verification, development and improvement of the hydrological model, land surface process model and climate model on the QTP. The datasets are available from the National Tibetan Plateau/Third Pole Environment Data Center (https://data.tpdc.ac.cn/en/disallow/789e838e-16ac-4539-bb7e-906217305a1d/, doi: 10.11888/ Geocry.tpdc.271107).

1 Introduction

Permafrost is widely distributed on the QTP, which is called the "Third Pole of the Earth" (Qiu, 2008), is about 1.06×10^6 km^2 in area and accounting for approximately a quarter of the QTP (Zou et al., 2017). Its unique and complicated hydrothermal process has great regulating effects on ground surface moisture, energy and mass exchange, ecosystem stability and carbon cycles (Cheng et al., 2019; Schuur et al., 2011). The surface energy and water cycle over the QTP have great influence on Asian monsoon, East Asian atmospheric circulation and global climate change (Ma et al., 2017; Yao et al., 2017). The characteristics of diabatic heating field of QTP are also used as an important factor for the short-term climate prediction in China (Liu and Hou, 1998; Wu et al., 2009; Ye and Gao, 1979).

The permafrost in the QTP has experienced significant degradation in response to climate warming, which mainly manifested as the permafrost area shrinking and ground temperature (GT) rise, the increased active layer, and decreased permafrost thickness (Hu et al., 2019b; Sharkhuu et al., 2007; Wang et al., 2000; Cheng et al., 2019). The permafrost degradation has caused changes in surface vegetation characteristics. It was reported that the area of Alpine meadow on the QTP decreased by 16.2×10^4 km^2 (accounted for 32.4% of the QTP (Zhao and Sheng, 2015)) in recent decades, which caused the change in hydrological processes and ecological environment and further led to desertification (Cheng and Jin, 2013; Cheng et al., 2019; Wu et al., 2003; Zhao et al., 2019). In addition, permafrost degradation could result in the decomposition of organic matter and greenhouse gases increased, which will finally affect the surface energy balance and the climate system (Wang et al., 2006a; Ping et al., 2015; Schuur et al., 2015; Schuur et al., 2011; Wu et al., 2012; Hu et al., 2019a). Permafrost degradation has also altered the geomorphological features and affected the stability of engineering structures in this region (Zhao et al., 2017).

However, the collection of long-term and high-resolution data over the permafrost regions of QTP is challenging due to the complex terrain, severe weather, and inconvenient access (Ma et al., 2008; Li et al., 2012). Previous studies on the permafrost focused on local and site scale and major along the Qinghai-Xizang Highway (QXP)/Railway (Cuo et al., 2015; Su et al., 2013). Some new observation sites in permafrost regions in the vast western territory of the QTP were reported in recent years (Zhao et al., 2017; Zhao et al., 2018; Zhao et al., 2020). Nevertheless, the climate background used in almost all the permafrost studies was based on the only 4 national meteorological stations located within the vast territory of permafrost regions. It is urgent to establish a synthesis observational database of permafrost thermal state and its climatic background to satisfy the requirements of calibration and validation for remote sensing interpretation and hydrothermal processes simulation, and also for the key parameters acquisition in permafrost regions (Bao et al., 2016; Li and Koike, 2003; Wang et al., 2017; Zhang et al., 2008; Hu et al., 2020). The complexity of the dynamic process of water and heat in freeze-thaw cycles is also considered one of the crucial reasons for the great errors in permafrost change simulation (Chen et al., 2014; Hu et al., 2016; Yang et al., 2018). Nevertheless, it is of great significance to provide a set of data in dynamic thermal characteristics of the permafrost on the QTP (Wang et al., 2006b; Zhao et al., 2004).

The Cryosphere Research Station on the QTP, Chinese Academy of Sciences (CRS-CAS), has established a comprehensive and widely permafrost monitoring network on the QTP (Zhao et al., 2019, 2020). This network mainly focuses on monitoring permafrost and its environmental factors in high-elevation and cold-climate regions of the QTP. Since the station was established in 1987, we have conducted long-term continuous monitoring and large-scale field investigations on permafrost. Thus, it synthetically studied the mechanisms of the change in hydrothermal conditions permafrost and their simulations and ecological effects. This paper firstly integrated air temperature, GT, soil moisture and permafrost temperature dataset over the permafrost regions across QTP from the CRS-CAS monitoring networks. The monitoring network is summarized in Sect. 2. In Sect. 3, the datasets are described in detail. In Sect. 4, the data availability and access are provided, and in Sect. 5, the conclusions and future work are summarized.

2 Monitoring networks and data processing

2.1 Permafrost monitoring networks

The vegetation in the permafrost region of the QTP is mainly alpine meadow, swamp meadow, alpine steppe, and alpine desert (Wang et al., 2016). The soils in the western permafrost region are Gelisols, Inceptisols and Aridisols, and in the eastern mainly consists of Gelisols, Mollisols and Inceptisols (Li et al., 2015). The permafrost monitoring network includes 6 automatic meteorological stations (AMSs), 12 active layer sites and, 84 boreholes (Fig. 1, Table 1), which were primarily selected based on the landforms and underly surface conditions (e.g., the vegetation and soil characteristics) along the Qinghai-Xizang Engineering Corridor and in each investigated region of the QTP. The elevation of all the sites is higher than 4000 m a.s.l (31.82~37.75 °N, 77.58~99.50 °E).
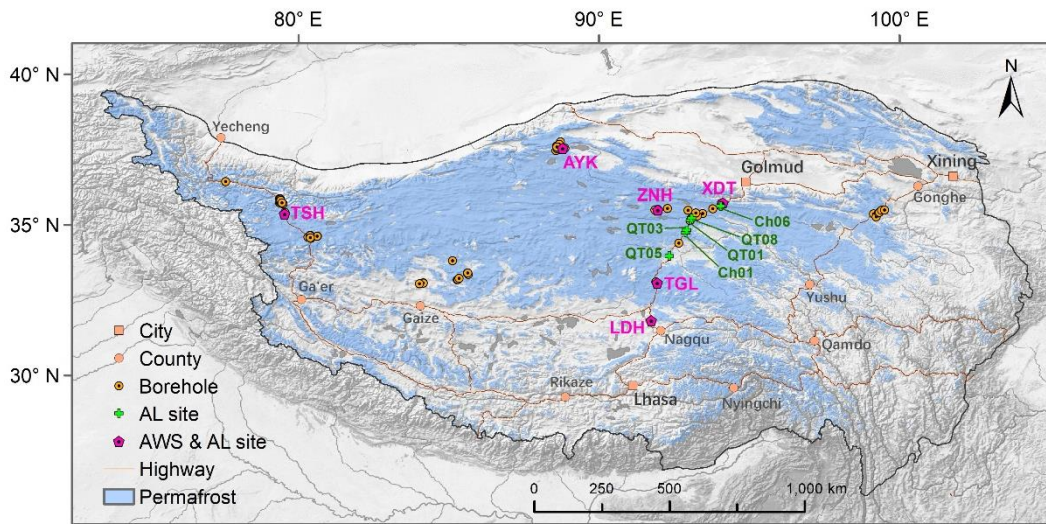
Figure 1. The permafrost monitoring networks on the QTP. AL: active layer; AWS: automatic meteorological

station

We set 6 AMSs (Fig. 2) within the permafrost zone since 2004. The main observation indices include air temperature, humidity, wind speed gradient observation, radiation balance, and precipitation, etc. The active layer observation system and GT borehole were set up simultaneously to record the permafrost, climate, vegetation, soil indices in different regions of the QTP. Liangdaohe (LDH) site has the lowest latitude, and it gets the warmest air temperature and the largest annual precipitation, while Tianshuihai (TSH) and Ayake (AYK), located in the northwest and north of the QTP, respectively, have the minimum and penultimate temperatures and annual precipitations. TSH has the highest solar radiation among the 6 stations.

Xidata (XDT) and Tanggula (TGL) are two sites with the most extended sequence of 6 gradient

meteorological stations. They were established in May 2004 and data sequences are over 16 years. XDT is located near the northern permafrost boundary of the QTP, and represents the characteristics of the island permafrost. TGL site is located on the north side of the Tanggula Mountains in the hinterland of the QTP and represents the characteristics of the continuous permafrost area. LDH is located near the southern boundary of the permafrost region and represents the characteristics of the discontinuous permafrost region. ZNH is located in the Hoh Xil region, where there was no meteorological station and even no in situ meteorological monitoring data ever before. It fills the data gap in the central and northern areas of the QTP and is also located in a continuous permafrost area. AYK is located in the Altun Mountains area in the northern Tibetan Plateau, a vast unmanned area on the QTP, and is one of the areas with few observations. TSH is located in the West Kunlun Mountain area near the western border of the permafrost region on the QTP. It can reflect the regional characteristics of arid, cold, and high altitude in the vast western part of the QTP. The GT and soil moisture observed of the active layer and permafrost were summarized in Table 1.
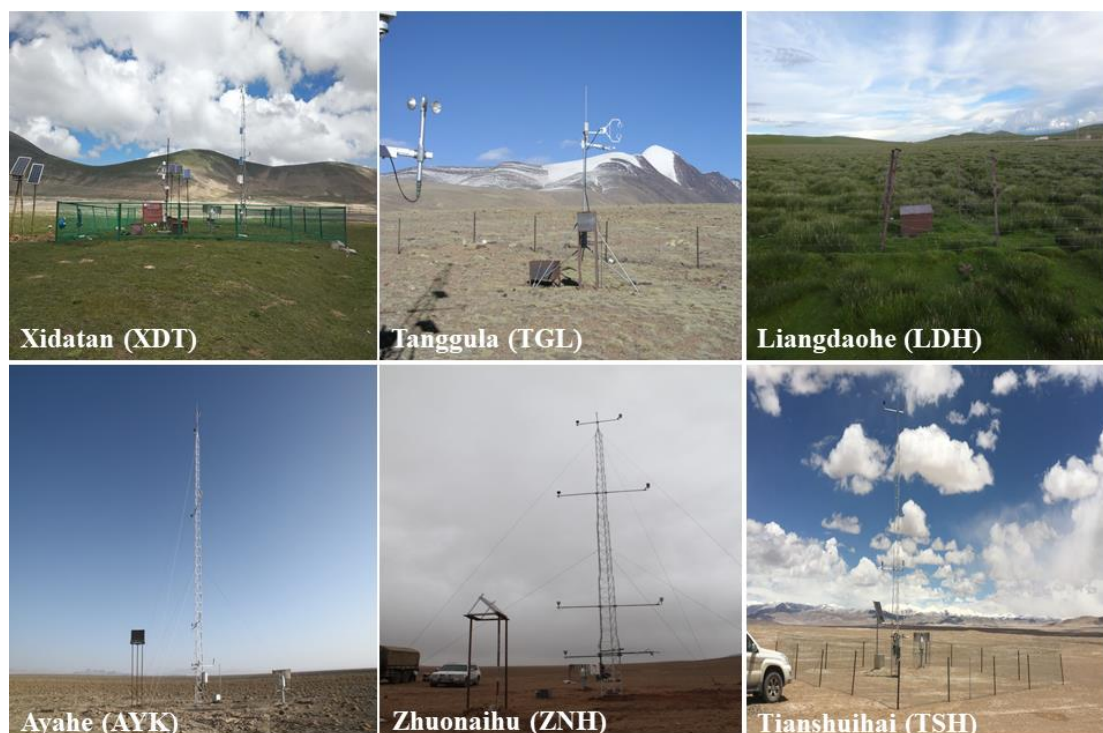
Figure 2. The six comprehensive meteorological stations

Table 1 The observation instruments and items for meteorological data, ground temperature and soil water content

Observation site type	Available sites	Observation item	Instrument	Accuracy	Height/Depth	Frequencies
Meteorological Stations	6	Upward/downward short-wave radiation	CM3, Kipp & Zonen, Holland	±10%	2 m	1/2 hour

		Upward/downward long-wave radiation	CM3, Kipp & Zonen, Holland	±10%	2 m	
		Air temperature	HMP45C, Vaisala Finland	±0.5 ℃	2,5,10 m	
		Air humidity		±3% RH	2,5,10 m	
		Wind velocity	05103_L/RM, Campbell, USA	±0.3 m/s	2,5,10 m	
		Precipitation	T-200B Precipitation Gauge	±0.1 mm	5 m away	
Active Layer	12	Soil temperature	105T/109 Thermocouple temperature sensor	±0.1 ℃ ±0.2 ℃	0.5 m,1.0 m,2 m, >2 m	1/2 hour
		Soil moisture content	CS616/ Hydra Soil moisture sensor	±2.5%		
Borehole (automatic)	15	Ground Temperature	Thermistor, SKLFSE, CHINA	±0.05 ℃	3, 6, 10, 20 m	1 hour
Borehole (manual)	69	Ground Temperature	Thermistor, SKLFSE, CHINA	±0.05 ℃	10, 20 m	1 year

129 **2 Monitoring data**

130   The main observation items and instruments for the meteorological observations were shown

131 in Table 1. The observation was done every 10 minutes and was averaged and recorded every 30

132 minutes automatically. The data were recorded by CR10X, CR1000 and CR3000 data logger

133 (Campbell Scientific). Meteorological data (e.g., the precipitation, radiation, air temperature,

134 relative humidity and wind speed) were recorded hourly with a CR1000/CR3000 data acquisition

135 instrument (Campbell Scientific Inc., USA) (Fig 3a). There were three measured at heights of 2 m,

136 5 m and 10 m for air temperature, relative humidity and wind speed (Table 1).
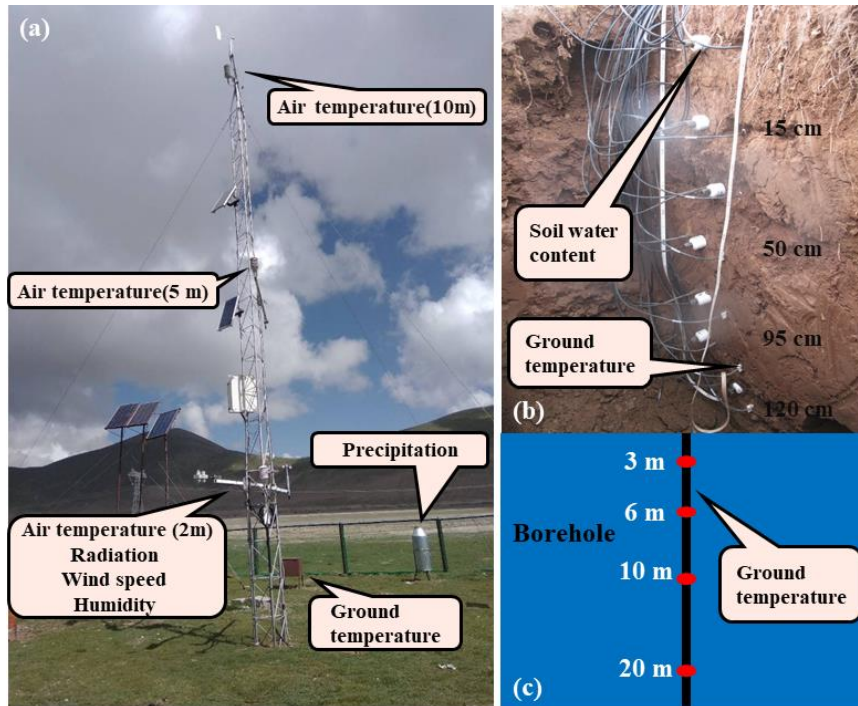
Figure 3. The comprehensive observation system**:** (a) meteorological observation, (b) ground temperature and soil water content in the active layer and (c) ground temperature observation for permafrost.

The GT for the active layer monitoring system was measured at different depths from ground surface to the depth of 10 to 50 cm below the permafrost table with a 105T/109 thermocouple Probe with an accuracy of ± 0.1 ℃/± 0.2 ℃ in the active layer (Fig 3b). The soil water content was measured by a Hydra soil moisture sensor (Table 1) by connecting to a CR10X/CR1000/CR3000 data logger (Campbell Company, USA).

The GT in the borehole was measured by the Thermistor (with an accuracy of ± 0.1 ℃) produced by the State Key Laboratory of Frozen Soil Engineering, Cold and Arid Regions Environmental and Engineering Research Institute of the Chinese Academy of Sciences (SKLFSE, CAREERI, CAS), which were downloaded to the depths of 3 m, 6 m, 10 m and 20 m depths within a steel pipe in the boreholes. All the borehole GTs along the QXH and located at the same sites with AMSs were measured at 15 minutes. The averaged value for each hour was automatically recorded by data loggers (CR1000/ CR3000, Campbell Scientific Company, Logan, UT, USA). Moreover, all the other boreholes far away from the QXH were measured manually by a digital multimeter once for one or two years according to the local transportation, financial supports, etc. (Table 1) (Fig 3c).

2.3 Data processing workflow

156   The data processing workflow is showed in Fig. 4. The quality control was two-fold: (1) the

157   missing data were replaced by -6999; (2) the singular unphysical data were rejected, and the gaps

158   were replaced by -6999. In addition, all the daily data were calculated by every 30 min (1 h) interval

159   per day for the data collected by data loggers. The instruments at meteorological stations are

160   calibrated every few years by comparing observations with standard instruments for about one week.

161   The active layer thickness was derived by the maximum depth of 0 ℃ isotherms from linear

162   interpolation of the daily maximum GT. The monthly and annual mean air and GTs, radiation, wind

163   speed, relative humidity and soil water content were also analyzed. The trend of air temperature,

164   active layer thickness, and GT is analyzed and provided at the stations with long-time observation.

165   GTs from manually monitoring boreholes were quality controlled for every measurement.
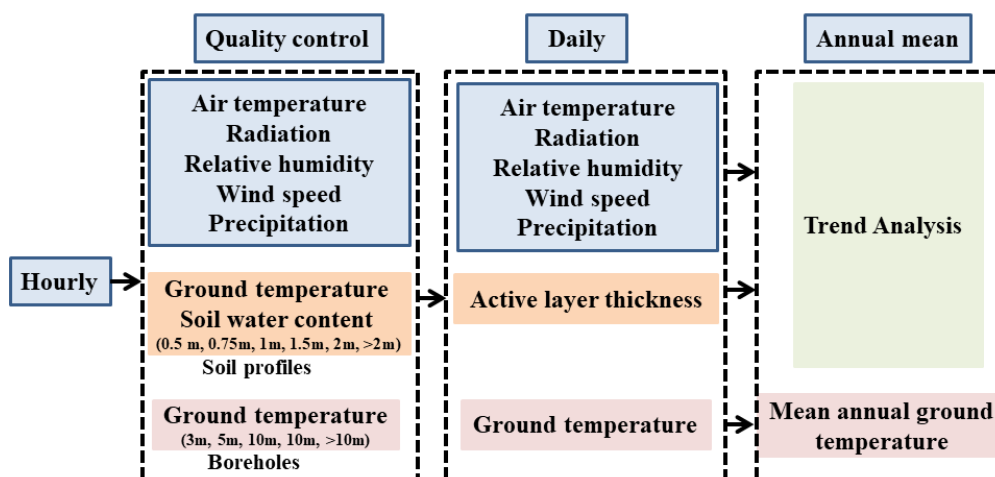
167   **Figure 4**. Schematic diagram of data processing workflow used to compile the permafrost dataset on the QTP.

3 Data description and evaluation

3.1 Meteorological data

Table 2. The information of six meteorological stations

Sites	XDT	TGL	LDH	ZNH	AYK	TSH
Latitude (ºN)	35.72	33.07	31.82	35.49	37.54	35.62
Longitude (ºE)	94.13	91.94	91.74	91.96	88.8	94.06
Elevation (m a.s.l)	4538	5100	4808	4784	4300	4844
Vegetation	Alpine steppe	Alpine meadow	Alpine wet meadow	Alpine desert	Alpine desert	Alpine desert

steppe

Observation height above the ground surface (m)	2,5,10	2,5,10	2,5,8	2,4,10,15	2,4,10,15	2,4,10
Data since	2004.5	2004.5	2014.9	2013	2013	2015
Missing date	17.7~17.9	09.6~09.8, 16.10~17.9, 17.12~18.1,	18.1~18.4	14.7~15.4 (Ta, Preci.)	15.8~15.9	Ws at 2m
Ta (°C)	-3.6	-4.7	-2.3	-4.9	-5.2	-6.0
RH (%)	53.5	51.5	48.2	53.9	46.1	40.6
Precipitation (mm)	384.5	352.0	388.6	277.8	158.6	103.3
Wind speed (m/s)	4.1	4.1	3.2	4.7	4.5	
DSR (W/m^2)	224.2	233.4	231.4	204.8	198.2	250.8
USR (W/m^2)	66.8	61.4	46.6	46.3	53.8	68.5
DLR (W/m^2)	223.0	214.8	237.2	233.8	223.0	211.5
ULR (W/m^2)	304.5	304.5	315.9	303.2	307.6	311.3
Net radiation	75.9	82.3	106.0	89.2	59.8	82.5

The seasonal variation of air temperature at all 6 sites is significant with the annual mean from -2.3 to -6 °C (Fig. 5). The mean monthly air temperatures in summer are positive but are lower than 0 °C in the other 3 seasons. The differences in the air temperatures between 6 stations were minimal in summer, evident in spring and autumn, and much prominent in winter, mainly caused by the difference in altitude and latitude.

Significant seasonal variation of precipitation is closely related to the monsoon cycles. From May to September, precipitation accounts for more than 85% of its annual amounts at the 5 sites other than TSH (78.6%). Most of the precipitation is concentrated in summer. A small amount is in late spring and early autumn and rare in the winter. Precipitation has a significant spatial difference, which is more than 350 mm on average at XDT, TGL, LDH along QXH. The precipitation at ZNH, located in the hinterland of the QTP and about 200 km from the QXH, is slightly lower, while it is

181   about 150 mm (slightly higher than half at ZNH) in AYK, which is located on the northern edge of

182   the QTP and has the highest latitude among all the 6 sites. The annual total precipitation at TSH,

183   located near the western boundary of QTP, is the lowest of all the observation sites and is only 100

184   mm.

185   The seasonal variation of air humidity is very consistent with the seasonal variations in air

186   temperature and precipitation. The difference between the stations is related to the precipitation,

187   especially in summer. Due to the scarce precipitation, the relative humidity at TSH and AYK is low

188   throughout the year. It is worth noting that the relative humidity in TGL and LDH is quite low in

189   winter due to these 2 sites are located in relatively lower latitude compared with the other 4 stations.

190   The air temperatures in winter at these 2 stations are relatively higher. The wind speeds at all stations

191   are generally high except LDH. The average annual wind speeds are higher than 4 m/s. The wind

192   speed is the highest in winter, followed by spring and the lowest in summer. The wind speed of

193   LDH was the lowest throughout the year in all AMSs, primarily due to its geomorphological

194   location, as it is a well-developed basin covered with swamp meadow.

195   Downward short-wave radiation (total solar radiation) usually reaches its maximum in May

196   and decreases in summer due to rainy- and cloudy-day influences at most sites except TSH. The

197   mean downward short-wave radiation in summer is only slightly higher than that in spring. However,

198   at TSH (with little precipitation), it is very high in summer and significantly higher than other sites

199   in spring and autumn. The upward short-wave radiation is mainly restricted by the surface albedo.

200   Its high value mainly appeared in autumn and indicated that snow falling events mainly occurred in

201   autumn, followed by spring and relatively little in winter. The upward short-wave radiation of TSH

202   in all seasons is high, related to dry and "snow-like" salt-rich ground surface caused by low

203   precipitation but very high evaporation. The upward and downward long-wave radiation is closely

204   related to air temperature and surface temperature, respectively, and their seasonal variation trend

205   is basically consistent with the change of air temperature.
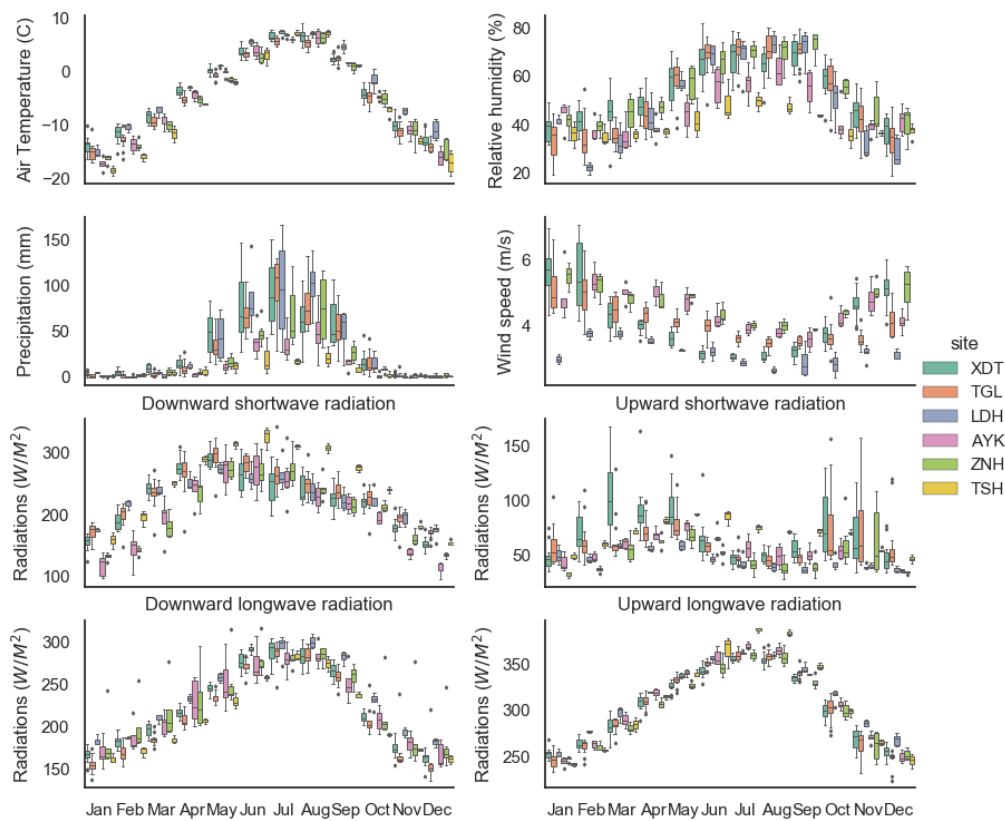
Figure 5. Characteristics of monthly observation variables at six meteorological stations

XDT and TGL stations had the data series with a longer period (from 2004 then) and can provide basic data for physical process research and land surface process model research. The annual mean temperature of the two stations showed increasing trends, with rates of 0.66 and 0.40 °C/10a, and p-values of 0.27 and 0.23, respectively. The warming trend is the highest in summer and autumn. However, the air temperature in winter shows a slight decrease. The precipitations show an insignificant week decrease trend (-15.0 and -14.3 mm/10a). It shows a slightly decreasing trend in summer and autumn and an increasing trend in spring (Fig. 6). The changing trend in air temperature and precipitation from these 2 stations was almost entirely contrary to the results from previous researches, which might be due to the limited monitoring time series.
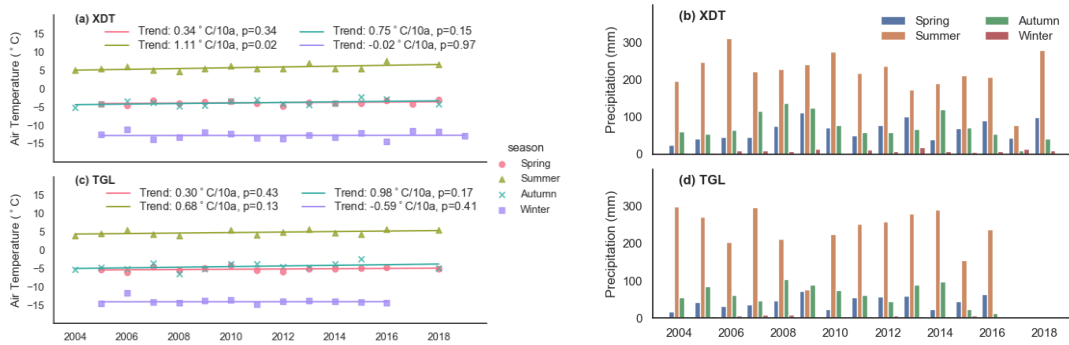
Figure 6. Seasonal mean series and changes of temperature and precipitation at XDT and TGL from 2004 to 2018

3.2 Active layer data

3.2.1 Variation of active layer thickness

The active layer thicknesses varied from about 120 cm to about 300 cm along Qinghai-Tibet highway under different surface vegetation conditions (Fig.7). Ch04, which locates at sporadic island permafrost of the QTB southern permafrost distribution limit regions under swamp meadow condition, appeared as the shallowest active layer site. Its average thickness was 116cm during the years 2000-2018. The deepest active layer appeared at QT05, which locates at the margin of permafrost from taliks formed by the thermal influences from the tributaries of Yangtze River headwaters, Tongtian river and Tuotuo river. Its average thickness was 307cm from 2004 to 2013, where the surface vegetation is alpine meadow. In the continuous permafrost zone of QTP, including Ch06, QT08, QT01, QT03, and Ch01 sites, the shallowest active layer is located at the Kunlun Mountains pass (Ch06) under nearly bare land surface vegetation condition with an average thickness of 147 cm during 2005-2018. The deepest active layer is located at Wudaoliang (QT08) under bare land with an average thickness of 235 cm during 2010-2018. For representative alpine meadow conditions (e.g., QT01 at Wudaoliang and Ch01 at Fenghuo Mountains), their average thicknesses were 163 cm and 167 cm. While at Beiluhe (QT03), about 10 km north of Ch01 site, its average thickness was about 231 cm with typical alpine meadow condition, which is larger than QT01 and Ch01. In addition, the QT09 called Xidatan is located at the north boundary of the permafrost region with an average active layer thickness of 141cm during 2011-2018 under typical alpine meadow conditions. Overall, in our opinion, the ground surface vegetation conditions may

240 have some influences on active layer thickness spatial distribution. However, it is not a controlling
241 factor, especially at a large spatial scale. The spatial distribution of active layer thickness was jointly
242 influenced by climate conditions, GT (including ground surface temperature and permafrost layer
243 temperature), soil water content, soil texture. Due to the great spatial variation of these above
244 influencing factors, the active layer thickness within our monitoring regions presented as a great
245 spatial variation.

246   In terms of time variation, all the monitoring sites showed the same pattern. Their active layer
247 thicknesses were increasing gradually. Their increasing rate was very different from sites, with the
248 largest increasing rate of 3.9 cm/yr at Ch01 and the lowest increasing rate of 0.8 cm/yr at QT05. Of
249 which worth noting is that the active layer thickness increasing rate is susceptible to the statistical
250 period. For instance, the average increasing rate of QT09 was 3.0 cm/yr during 2011-2018. While
251 during 2014-2018, its average increasing rate was 6.9 cm/yr. Thus, the increasing statistical active
252 layer thickness rates cannot be considered a long-term thickness increasing trend. It only revealed
253 that the active layer thickness has a slow increase trend with inter-annual fluctuation, and their
254 increasing amplitudes are very different amount different monitoring sites.
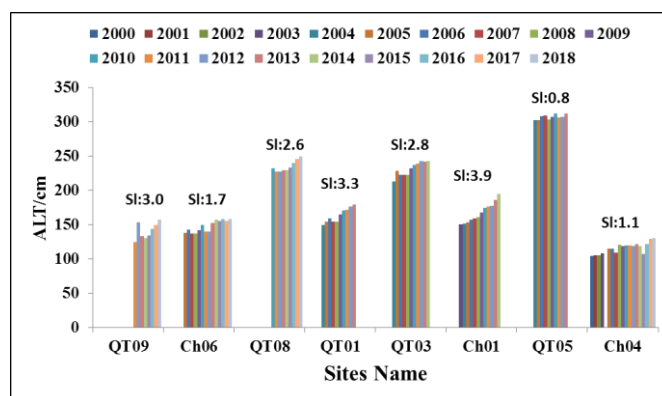
256 **Figure 7**. Variation in active layer thickness among different sites. SI represents the active layer thickness average
257 annual increasing rate.

3.2.2 Temperature in the active layer

259   In this section, we choose GT at 10cm depth and the base of the active layer from 2011 to 2013,
260 during which continuous GT monitoring data series of all eight active layer monitoring sites were
261 available, to analyze the active layer GT spatial distribution and their influence on active layer
262 thickness spatial distribution (Table.3). The GT (ALT_Base_GT) was derived from geothermal

interpolation when there was no temperature probe at the actual active layer depth position at the base of the active layer. For all 8 active layer monitoring sites, the mean annual GT (10 cm_GT) varied greatly from site to site at 10cm depth. The lowest 10 cm_GT appeared at Kunlun Mountains region (Ch06), which is -2.86 ℃. For QT03, QT05 and Ch04, the 10cm_GT were positive and as high as 1.12 ℃ and 1.25 ℃ at sites QT05 and Ch04. For ALT_Base_GT, the relatively low temperature all appeared at mountain regions, such as Ch06 at the Kunlun Mountains and Ch01 at Fenghuo Mountains. This because the ALT_Base_GT was simultaneously influenced by ground surface temperature and underlain permafrost temperature, and in mountains regions, the permafrost layer temperature is often very low in QTP. At the marginal regions of permafrost distribution or island permafrost, such as QT09, QT05 and Ch04, the ALT_Base_GT were relatively higher than other sites due to their high underlain permafrost layer temperature.

Table. 3 The mean active layer thickness, ground temperature at depth of 10 cm and permafrost table

Sites Name	ALT/cm	10cm_GT/℃	ALT_Base_GT/℃
QT09	137	-1.3	-1.34
Ch06	146	-2.86	-2.68
QT08	228	-1.64	-1.45
QT01	176	-1	-1.7
QT03	241	0.03	-1.29
Ch01	180	-1.35	-2.47
QT05	308	1.12	-0.17
Ch04	120	1.25	-0.51

The scatter plot between active layer thickness and 10cm_GT showed that, on the whole, ALT increased with the increase of 10cm_GT, but they are not linear dependent (Fig.8a). Especially for Ch04 at island permafrost region under swamp meadow surface vegetation, the relationship between ALT and 10cm_GT was very different from other monitoring sites, demonstrating that surface GT spatial distribution did influence ALT distribution. However, it cannot be used as a primary control factor for ALT prediction under different soil and vegetation conditions. In contrast to the relationship between ALT and 10 cm_GT, the relationship between ALT and ALT_Base_GT is much better (Fig.8b). If without considering the large deviation of sites QT09 and Ch04, active layer

283 thickness was nearly linear dependent on the variation of ALT_Base_GT, which indirectly showed

284 that the underlain permafrost temperature properties have a great influence on ALT distribution.
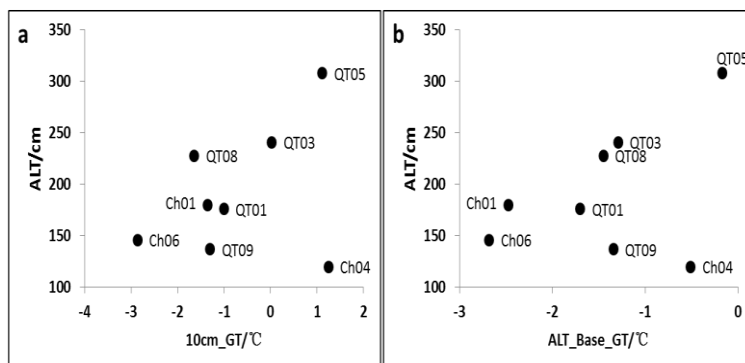
286 **Figure 8.** The relationship between active layer thickness and the temperature of the permafrost table

287 The shallow GT of 8 active-layer monitoring sites was collected with automatic data loggers

288 along the Qinghai-Tibetan Road in the dataset. The 10-cm annual mean GT was ranged from -2.62 ℃

289 to -0.20 ℃ for all sites, while ranged from -2.69 ℃ to -0.37 ℃ near the top of the permafrost. The

290 temperature at two depths has a good linear correlation. The mean GTs near the top of permafrost

291 at 6 sites were 0.30 ℃ to 1.83 ℃ lower than that of 10 cm. At only 2 sites (CN06 and QT08), the

292 former is slightly higher than the latter (approximately 0.2 ℃). The subsurface GT of 10 cm at all

293 the sites showed increasing trends with increased rates ranging from 0.03 ℃ to 0.19 ℃ per year.

294 The maximum rate occurred at site QT09 which locates the northern marginal region of permafrost.

295 The increasing rate at the bottom of the active layer (near top of permafrost) is slightly lower than

296 the rate of surface active layer. Even at CN06, there was a slight cooling trend at the bottom of the

297 active layer.

3.2.3 Soil moisture in the active layer

299 The average volumetric soil water content (VWC) within ALT was calculated with a depth-

300 weighted average method when the ground surface began to freeze and ALT reached its max

301 thawing depth at each monitoring site (Fig.9a). In terms of inter-annual change, VWC had no

302 obvious changing trend with random inter-annual fluctuations. In terms of spatial variation, the

303 VWC varied from 0.141 to 0.403 m^3/m^3 among our monitoring sites, with the largest VWC at Ch04

304 and the lowest at QT08. Active layer soil water content was basically controlled by ground surface

305 vegetation conditions, soil texture and local drainage conditions. For example, a swamp meadow at

306 Ch04 with about 60 cm depth of peat soil layer beneath the ground surface resulted in the very

307 shallow active layer thickness and nearly saturated soil water content condition. At QT05, the soil

308 pit excavated in 2007 revealed that it was sand within 140cm. This site has terrible drainage

309 conditions and resulted in relatively high VWC, averaged 0.292 m^3/m^3 during 2004-2018. While at

310 QT08, where the soil type is also sand within the active layer, because of its excellent drainage

311 conditions, VWC is very low, averaged 0.141 during 2012-2018.

312   Converting the VWC into total soil water depth per unit area stored within the active layer, soil

313 water depth varied from 290 mm to 890 mm among our monitoring sites (Fig.9b). QT05 had the

314 highest soil water depth, averaged 890 mm during 2004-2008. High soil water depth must absorb

315 high heat energy during the active layer thawing process, explaining why the active layer thickness

316 increasing rate was very low, while its ground surface temperature was very high.
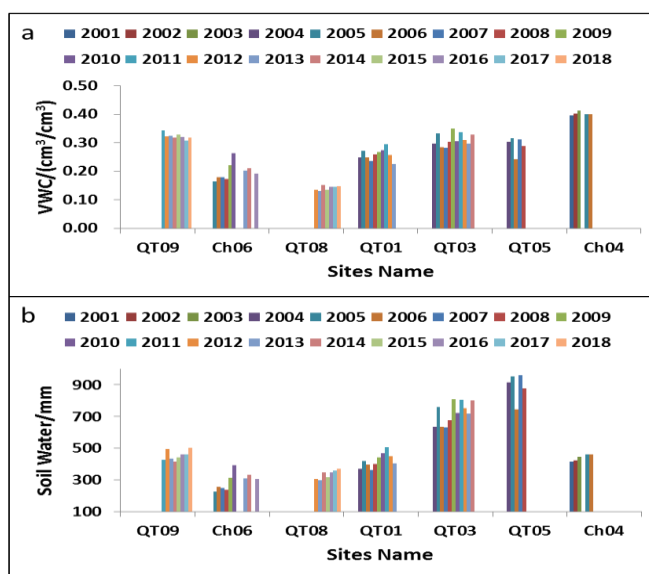
317

318   **Figure 9.** Variation in volumetric water content and soil water equivalent among different sites

319 ## 3.3 Permafrost temperature

320   Fifteen borehole sites automatically collected GT at different depths; 14 are located in the

321 permafrost regions and only one is located in a structural talik region (QTB11). Annual mean GTs

322 at depths of 3 m and 6 m are given. The GT of these two horizons at most sites has obvious seasonal

323 variation and has remarkable inter-annual variation. Except for QTB11 locating in the seasonally

324 frozen ground region, the available mean annual GTs at 10 m and 20 m are shown in Fig. 10. For

325 the temperature of 10 m, the highest permafrost temperature appears at site QTB05 that locates in

326 the Qumar River along the Qinghai-Tibetan Road, the mean annual GT of which is very close to

327 0 ℃. Meanwhile, the active layer thickness has approximately exceeded 9 m. The lowest

328 temperature appears at site FCKGT that locates in a high plain area in the south of Altun Mountain,

329 where the permafrost temperature reaches -4 ℃ due to extremely cold and dry climatic conditions.

330 The GT at all 15 boreholes showed significant linear increasing trends, and the permafrost has

331 warmed at different rates (Fig. 10). The warming rates at a depth of 10 m was ranged from

332 0.02 ℃/decade (FCKGT) to 0.78 ℃/decade (QTB05) but varied between 0 ℃/decade and

333 0.24 ℃/decade at a depth of 20 m. The annual mean temperature of 20 m at site ZNHGT has rarely

334 changed during 2013-2018. At this depth, the most significant warming occurred at site QTB02,

335 QTB18 and QTB15.
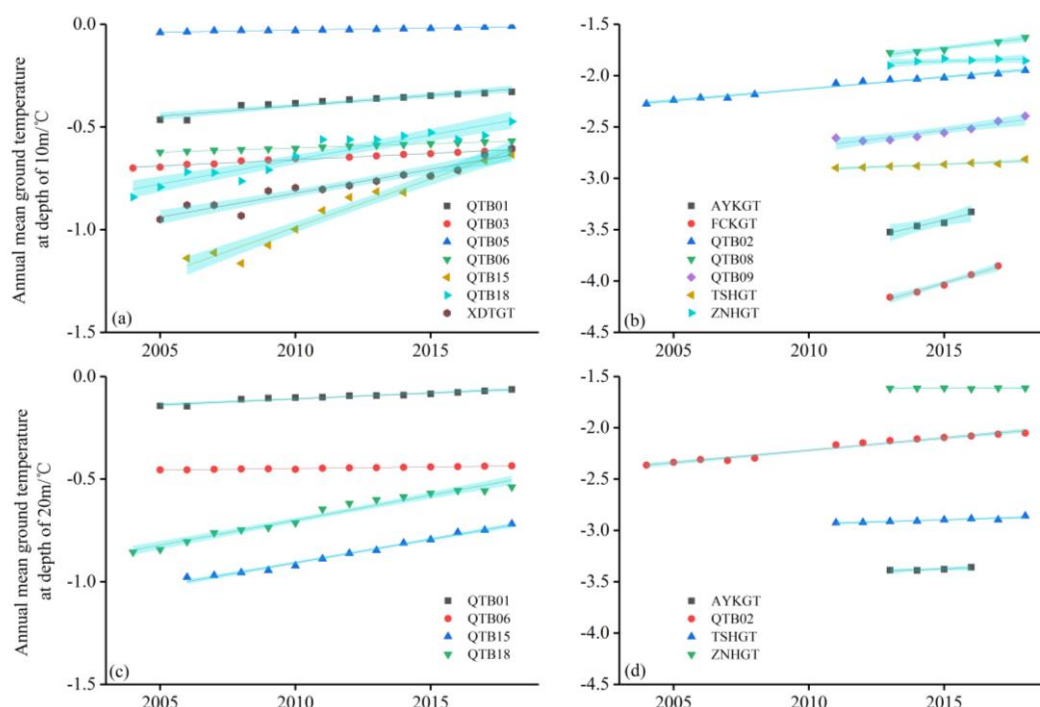
336

337 **Figure 10.** Annual mean ground temperature as a function of time at a depth of (a, b) 10 m and (c, d) 20 m from

338 borehole with continuous data series

339   The warming rate of permafrost seems to have a strong relationship with the temperature of

340 permafrost itself. Fig. 11a shows that the change rate of GT at two shallow depths (10 cm and the

341 depth near top of permafrost). They show an increasing trend first and then decreasing as the

342 temperature near the bottom of the active layer rises. Both colder and warmer sites have a relatively

343 lower variation rate of GT. The sites with GTs between -2 ℃ and -1 ℃ have the greatest ground

344 warming rate. The warming of the active layer in permafrost regions may be mainly related to

regional climate and local topography. Because most sites (QT1,QT3,QT8) with the largest warming rates are located on the high plain in the interior of the QTP, and they are geographically relatively close to each other. The two sites (CN1,CN6) with the lowest GT are located in the mountain areas (respectively belong to Fenghuo Mountain and Kunlun Mountain). At the same time, the other two sites (CN4, QT5) with the highest GT are located in the regions with the warmest climatic conditions, although the underlying surfaces are substantially different. Further study is necessary because the current number of sites is far from enough.

However, the deep GT shows another pattern and lower temperature permafrost tend to have a great warming rate (Fig. 11b). It is consistent with the previous research at the QTP, and the correlation between permafrost temperatures and warming rates is more significant than the previous. It indicates that the ice-water phase transition effect in the conversion from permafrost to melting soil has significantly slowed GT increase.

We also analyzed another 69 sites, of which the GTs were recorded manually. The altitude of these sites ranges from 4142 to 5247 m a.s.l. The drilling depth of the borehole reached 10 m at most of the sites, and several reach 20 m. The observation interval is once every one year or two years., the multi-year averages based on single observations are calculated to compare the thermal regime of different sites. The multi-year mean GT of 10 m observed at different sites ranged from -3.84 ℃ to 3.36 ℃. There are 10 observation fields with a positive mean GT of 10 m and 59 fields with negative values. The site with the highest GT is HT01, and the one with the lowest temperature is STG. For all observation sites, the GT shows a slightly downward trend as the elevation increases.

365
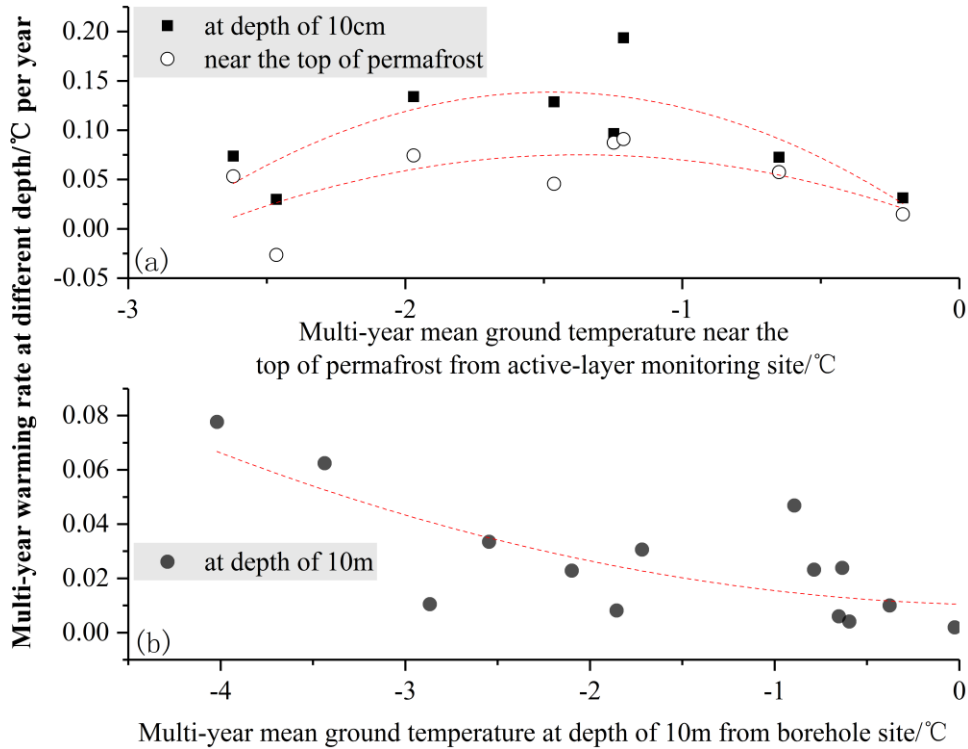
Figure 11. The relationship between warming rate and multi-year mean ground temperature during observation period from (a) active-layer monitoring site and (b) borehole site.

4 Data availability

All datasets in this paper have been released and can be free download from the National Tibetan Plateau/Third Pole Environment Data Center (https://data.tpdc.ac.cn/en/disallow/789e838e-16ac-4539-bb7e-906217305a1d/,doi: 10.11888/Geocry.tpdc.271107) or Cryosphere Research Station on Qinghai-Xizang Plateau (http://new.crs.ac.cn/).

5 Conclusions

The observation data in permafrost regions on the QTP can provide basic data for studying land-atmosphere interaction and climate change research. They could provide accurate inputs and verifications for land surface models, reanalysis data and remote-sensing products, and climate models. The results revealed that the annual mean air temperatures of all 6 sites are between -2.3 ~ -6 ℃, and their seasonal variation characteristics are significant. Precipitation shows a significant seasonal change trend, which is closely related to the monsoon period. The annual mean air temperature of the XDT and TGL stations showed increasing trends, with rates of 0.66 and 0.40 ℃/10a, respectively, and the GT has significant warming trend. The precipitations show an

insignificant week decrease trend. The active layer thickness has a slow increase trend with inter-annual fluctuation, and their increasing amplitudes are very different amount different monitoring sites. In addition, the high-quality comprehensive dataset with a focus on permafrost thermal state on the QTP could provide accurate and effective forcing data and evaluation data for different models. This valuable permafrost dataset is worth maintaining and promoting in the future due to hard-won. It also provides a prototype of basic data collection and management for other permafrost regions.

Author contributions. L Zhao generated and designed the observation network, participated in the field installation of most observation sites, found supports for maintaining the observation systems. DF Zou, GJ Hu, TH Wu, XD Wu, R Li, EJ Du, GY Liu, YP Qiao and X Yao participated in the field works and maintained the observation sites. GJ Hu, R Li, EJ Du, GY Liu, X Yao and DF Zou performed data processing, organization and analyses. GJ Hu, L Zhao, EJ Du, GY Liu, X Yao and DF Zou wrote the paper, and all authors participated in the revision of the manuscript.

Competing interests. No conflict of interest.

Acknowledgements. We would like to thank all the scientists, engineers, and students who participated in the field work and maintain this observation network and data acquisition.

Financial support. This work was financially supported by the National Natural Science Foundation of China (41931180), the Second Tibetan Plateau Scientific Expedition and Research (STEP) program, China (2019QZKK0201), and the National Natural Science Foundation of China (42071094, 41701073).

Reference:

Bao, H., Koike, T., Yang, K., Wang, L., Shrestha, M., and Lawford, P.: Development of an enthalpy-based frozen soil model and its validation in a cold region in China, J. Geophys. Res.-Atmos., 121, 5259-5280, https://doi.org/10.1002/2015jd024451, 2016.

Chen, B., Luo, S., Lu, S., Zhang, Y., and Ma, D.: Effects of the soil freeze-thaw process on the regional climate of the Qinghai-Tibet Plateau, Climate Research, 59, 243-257, https://doi.org/10.3354/cr01217, 2014.

Cheng, G., and Jin, H.: Groundwater in the permafrost regions on the Qinghai-Tibet Plateau and it changes, Hydrogeology & Engineering Geology, 40, 1-11, 2013.

Cheng, G., Zhao, L., Li, R., Wu, X., Sheng, Y., Hu, G., Zou, D., Jin, H., Li, X., and Wu, Q.: Characteristic, changes and impacts of permafrost on Qinghai-Tibet Plateau, Chinese Science Bulletin, 64, 2783-2795,

415   2019.

416   Cuo, L., Zhang, Y., Bohn, T. J., Zhao, L., Li, J., Liu, Q., and Zhou, B.: Frozen soil degradation and its
417   effects on surface hydrology in the northern Tibetan Plateau, Journal of Geophysical Research:
418   Atmospheres, 120, 8276-8298, https://doi.org/10.1002/2015JD023193, 2015.

419   Hu, G., Zhao, L., Wu, X., Li, R., Wu, T., Xie, C., Qiao, Y., Shi, J., Li, W., and Cheng, G.: New Fourier-
420   series-based analytical solution to the conduction-convection equation to calculate soil temperature,
421   determine soil thermal properties, or estimate water flux, International Journal of Heat and Mass
422   Transfer, 95, 815-823, https://doi.org/10.1016/j.ijheatmasstransfer.2015.11.078, 2016.

423   Hu, G., Zhao, L., Li A., R., Wu, X., Wu, T., Zhu, X., Pang, Q., Liu, G. Y., Du, E., Zou, D., Hao, J., and
424   Li, W.: Simulation of land surface heat fluxes in permafrost regions on the Qinghai-Tibetan Plateau
425   using   CMIP5   models,   Atmospheric   Research,   220,   155-168,
426   https://doi.org/10.1016/j.atmosres.2019.01.006, 2019a.

427   Hu, G., Zhao, L., Wu, X., Wu, T., Li, R., Xie, C., Xiao, Y., Pang, Q., Liu, G., Hao, J., Shi, J., and Qiao,
428   Y.: Variations in soil temperature from 1980 to 2015 in permafrost regions on the Qinghai-Tibetan
429   Plateau   based   on   observed   and   reanalysis   products,   Geoderma,   337,   893-905,
430   https://doi.org/10.1016/j.geoderma.2017.07.017, 2019b.

431   Hu, G., Zhao, L., Zhu, X., Wu, X., Wu, T., Li, R., Xie, C., and Hao, J.: Review of algorithms and
432   parameterizations to determine unfrozen water content in frozen soil, Geoderma, 368, 114277,
433   https://doi.org/10.1016/j.geoderma.2020.114277, 2020.

434   Li, R., Zhao, L., Ding, Y., Wu, T., Xiao, Y., Du, E., Liu, G., and Qiao, Y.: Temporal and spatial variations
435   of the active layer along the Qinghai-Tibet Highway in a permafrost region, Chinese Science Bulletin,
436   57, 4609-4616, https://doi.org/10.1007/s11434-012-5323-8, 2012.

437   Li, X., and Koike, T.: Frozen soil parameterization in SiB2 and its validation with GAME-Tibet
438   observations, Cold Regions Science and Technology, 36, 165-182, https://doi.org/10.1016/s0165-
439   232x(03)00009-0, 2003.

440   Liu, X., and Hou, P.: Relationship between the climatic warming over the Qinghai -Xizang Plateau and
441   its surrounding areas in recent 30 years and the elevation, Plateau Meteorology, 17, 245-245, 1998.

442   Ma, L., Zhang, T., Li, Q., Frauenfeld, O. W., and Qin, D.: Evaluation of ERA-40, NCEP-1, and NCEP-2
443   reanalysis air temperatures with ground-based measurements in China, J. Geophys. Res.-Atmos., 113,
444   https://doi.org/10.1029/2007jd009549, 2008.

445   Ma, Y., Ma, W., Zhong, L., Hu, Z., Li, M., Zhu, Z., Han, C., Wang, B., and Liu, X.: Monitoring and
446   Modeling the Tibetan Plateau's climate system and its impact on East Asia, Scientific Reports, 7,
447   https://doi.org/10.1038/srep44574, 2017.

448   Ping, C., Jastrow, J., Jorgenson, M., Michaelson, G., and Shur, Y.: Permafrost soils and carbon cycling,
449   Soil, 1, 147-171, https://doi.org/10.5194/soil-1-147-2015, 2015.

450   Qiu, J.: The third pole, Nature, 454, 393-396, https://doi.org/10.1038/454393a, 2008.

451   Schuur, E., McGuire, A., Schädel, C., Grosse, G., Harden, J., Hayes, D., Hugelius, G., Koven, C., Kuhry,
452   P., and Lawrence, D.: Climate change and the permafrost carbon feedback, Nature, 520, 171-179,
453   https://doi.org/10.1038/nature14338, 2015.

454   Schuur, E. A. G., Abbott, B., and Permafrost Carbon, N.: High risk of permafrost thaw, Nature, 480, 32-
455   33, https://doi.org/10.1038/480032a, 2011.

456   Sharkhuu, A., Sharkhuu, N., Etzelmüller, B., Heggem, E. S. F., Nelson, F. E., Shiklomanov, N. I.,
457   Goulden, C. E., and Brown, J.: Permafrost monitoring in the Hovsgol mountain region, Mongolia,
458   Journal of Geophysical Research Atmospheres, 112, 195-225, https://doi.org/10.1029/2006JF000543,

2007.

Su, F., Duan, X., Chen, D., Hao, Z., and Cuo, L.: Evaluation of the Global Climate Models in the CMIP5 over the Tibetan Plateau, Journal of Climate, 26, 3187-3208, https://doi.org/10.1175/JCLI-D-12-00321.1, 2013.

Wang, G., Li, Y., Wu, Q., and Wang, Y.: Impacts of permafrost changes on alpine ecosystem in Qinghai-Tibet Plateau, Science in China Series D: Earth Sciences, 49, 1156-1169, 2006a.

Wang, G., Li, Y., Wu, Q., and Wang, Y.: Impacts of permafrost changes on alpine ecosystem in Qinghai-Tibet Plateau, Science in China Series D-Earth Sciences, 49, 1156-1169, https://doi.org/10.1007/s11430-006-1156-0, 2006b.

Wang, L., Zhou, J., Qi, J., Sun, L., Yang, K., Tian, L., Lin, Y., Liu, W., Shrestha, M., Xue, Y., Koike, T., Ma, Y., Li, X., Chen, Y., Chen, D., Piao, S., and Lu, H.: Development of a land surface model with coupled snow and frozen soil physics, Water Resour. Res., 53, 5085-5103, https://doi.org/10.1002/2017wr020451, 2017.

Wang, S. L., Jin, H. J., Li, S. X., and Zhao, L.: Permafrost degradation on the Qinghai-Tibet Plateau and its environmental impacts, Permafrost and Periglacial Processes, 11, 43-53, 2000.

Wu, B., Yang, K., and Zhang, R.: Eurasian snow cover variability and its association with summer rainfall in China, Advances in Atmospheric Sciences, 26, 31-44, 2009.

Wu, Q., Shen, Y., and Shi, B.: The relationship between frozen soil together with its water-heat process and ecological environment in the Tibetan Plateau, Journal of Glaciology and Geocryology, 25, 250-255, 2003.

Wu, X., Zhao, L., Chen, M., Fang, H., Yue, G., Chen, J., Pang, Q., Wang, Z., and Ding, Y.: Soil Organic Carbon and Its Relationship to Vegetation Communities and Soil Properties in Permafrost Areas of the Central Western Qinghai-Tibet Plateau, China, Permafrost and Periglacial Processes, 23, 162-169, https://doi.org/10.1002/ppp.1740, 2012.

Yang, K., Wang, C., and Li, S.: Improved Simulation of Frozen-Thawing Process in Land Surface Model (CLM4.5), J. Geophys. Res.-Atmos., 123, 13238-13258, https://doi.org/10.1029/2017jd028260, 2018.

Yao, T., Piao, S., Shen, M., Gao, J., Yang, W., Zhang, G., Lei, Y., Gao, Y., Zhu, L., Xu, B., Yu, W., and Li, S.: Chained Impacts on Modern Environment of Interaction between Westerlies and Indian Monsoon on Tibetan Plateau, Bulletin of the Chinese Academy of Sciences, 32, 976-984, 2017.

Ye, D., and Gao, Y.: The Meteorology of the Qinghai-Xizang (Tibet) Plateau, Science Press: Beijing, 278 pp., 1979.

Zhang, Y., Carey, S. K., and Quinton, W. L.: Evaluation of the algorithms and parameterizations for ground thawing and freezing simulation in permafrost regions, J. Geophys. Res.-Atmos., 113, https://doi.org/10.1029/2007jd009343, 2008.

Zhao, L., Ping, C.-L., Yang, D., Cheng, G., Ding, Y., and Liu, S.: Changes of climate and seasonally frozen ground over the past 30 years in Qinghai–Xizang (Tibetan) Plateau, China, Global and Planetary Change, 43, 19-31, https://doi.org/10.1016/j.gloplacha.2004.02.003, 2004.

Zhao, L., and Sheng, Y.: Permafrost survey manual, Science Press: Beijing, 13-14 pp., 2015.

Zhao, L., Wu, T., Xie, C., Li, R., Wu, X., Yao, J., Yue, G., and Xiao, Y.: Support Geoscience Research, Environmental Management, and Engineering Construction with Investigation and Monitoring on Permafrost in the Qinghai-Tibet Plateau, China, Bulletin of the Chinese Academy of Sciences, 32, 1159-1168, 2017.

Zhao, L., Wu, X., Wang, Z., Sheng, Y., Fang, H., Zhao, Y., Hu, G., Li, W., Pang, Q., Shi, J., Mo, B., Wang, Q., Ruan, X., Li, X., and Ding, Y.: Soil organic carbon and total nitrogen pools in permafrost zones of

503   the Qinghai-Tibetan Plateau, Scientific Reports, 8, https://doi.org/10.1038/s41598-018-22024-2, 2018.

504   Zhao, L., Hu, G., Zou, D., Wu, X., Ma, L., Sun, Z., Yuan, L., Zhou, H., and Liu, S.: Permafrost Changes
505   and Its Effects on Hydrological Processes on Qinghai-Tibet Plateau, Bulletin of the Chinese Academy
506   of Sciences, 34, 1233-1246, 2019.

507   Zhao, L., Zou, D. F., Hu, G., Du, E., Pang, Q., Xiao, Y., Li, R., Sheng, Y., Wu, X., Sun, Z., Wang, L.,
508   Wang, C., Ma, L., Zhou, H., and Liu, S.: Changing climate and the permafrost environment on the
509   Qinghai–Tibet(Xizang) Plateau, Permafrost and Periglac Process, 1-10,
510   https://doi.org/10.1002/ppp.2056, 2020.

511   Zou, D., Zhao, L., Sheng, Y., Chen, J., Hu, G., Wu, T., Wu, J., Xie, C., Wu, X., Pang, Q., Wang, W., Du,
512   E., Li, W., Liu, G., Li, J., Qin, Y., Qiao, Y., Wang, Z., Shi, J., and Cheng, G.: A new map of permafrost
513   distribution on the Tibetan Plateau, Cryosphere, 11, 2527-2542, https://doi.org/10.5194/tc-11-2527-
514   2017, 2017.